Observation of sum-frequency-generation-induced cascaded four-wave mixing using two crossing femtosecond laser pulses in a 0.1 mm beta-barium-borate crystal

Weimin Liu, Liangdong Zhu, and Chong Fang*

Department of Chemistry, Oregon State University, Corvallis, Oregon 97331, USA
**Corresponding author: Chong.Fang@oregonstate.edu*

Received June 14, 2012; revised July 27, 2012; accepted July 30, 2012;
posted July 30, 2012 (Doc. ID 170478); published September 6, 2012

We demonstrate the simultaneous generation of multicolor femtosecond laser pulses spanning the wavelength range from UV to near IR in a 0.1 mm Type I beta-barium borate crystal from 800 nm fundamental and weak IR supercontinuum white light (SCWL) pulses. The multicolor broadband laser pulses observed are attributed to two concomitant cascaded four-wave mixing (CFWM) processes as corroborated by calculation: (1) directly from the two incident laser pulses; (2) by the sum-frequency generation (SFG) induced CFWM process (SFGFWM). The latter signal arises from the interaction between the frequency-doubled fundamental pulse (400 nm) and the SFG pulse generated in between the fundamental and IR-SCWL pulses. The versatility and simplicity of this spatially dispersed multicolor self-compressed laser pulse generation offer compact and attractive methods to conduct femtosecond stimulated Raman spectroscopy and time-resolved multicolor spectroscopy.

OCIS codes: 320.7110, 320.2250, 190.4380, 190.4160.

Over the past decade, broadband and wavelength-tunable femtosecond (fs) laser pulses from ultraviolet (UV) to mid-IR range have been developed using cascaded four-wave mixing processes (CFWM) in transparent bulk media (e.g., BK7 glass, fused silica and sapphire plate) [1–3], nonlinear crystals [e.g., beta-barium borate (BBO), $LiNbO_3$, $KNbO_3$, and $PbWO_4$] [4–7], and optical fibers [8–10]. By using two sufficiently intense fs laser pulses with a finite crossing angle in the medium, several frequency up- and down-converted pulses can be generated with good spatial separation [1,3–7]. These CFWM sideband signals are potentially suitable for applications in ultrafast time-resolved spectroscopy including multicolor transient absorption, microscopy, two-dimensional (2D) spectroscopy [11], and the recently developed femtosecond stimulated Raman spectroscopy (FSRS) to study molecular conformational dynamics [12].

In this work, which is different from the previously reported CFWM generations [1,3–7], we use two crossing fs near-IR (NIR) laser pulses to simultaneously generate two symmetric sets of CFWM signals with the broad wavelength range spanning from UV to NIR (350–1000 nm) in one thin 0.1 mm BBO crystal. These multicolor sideband signals are calculated and attributed to CFWM processes directly from the fundamental and IR-SCWL pulses, as well as the sum-frequency generation (SFG)-induced CFWM (SFGFWM) sideband signals occurring collinearly with the CFWM signal. These conveniently generated, spatially separated, and tunable self-compressed multicolor pulses make them attractive laser sources for time-resolved spectroscopy.

The experiment is performed using a fs laser system consisting of a mode-locked Ti:Sapphire oscillator and regenerative amplifier (Legend Elite, Coherent) that provides a 35 fs pulse centered at 800 nm with a 1 KHz repetition rate. After the beam splitter, one beam is focused on a 2 mm thick Z-cut single crystal sapphire to generate SCWL. The IR part of the white light with an 824 nm center wavelength is selected using an RG830 long pass filter (Newport), which is then compressed with a fused silica prism pair to produce the ~50 fs broadband IR pulse. The other much stronger beam (800 nm fundamental) passes through a delay stage and is attenuated by a variable neutral density filter. The two p-polarized beams are then loosely focused onto a 0.1 mm thick BBO (Type I, $\theta = 27.8°$) crystal. Both beam diameters on the crystal are ~0.2 mm. Pulse energy is ~3 μJ/pulse for the 800 nm and ~100 nJ/pulse for the IR-SCWL pulses, respectively. The crossing angle is ~6°. When we temporally and spatially overlap the two crossing laser beams with the BBO crystal rotated to the SFG phase-matching condition, multiple bright sidebands appear on both sides of the frequency-doubled fundamental (FDF) pulse at ~400 nm. So the observed SFGFWM signal in the UV-visible (UV-Vis) region can be attributed to second harmonic generation (SHG) + SFG assisted CFWM. We isolate and collect the different-order sideband spectra with an Ocean Optics spectrometer. To measure the fs pulse duration, we use a home-built, noncollinear SHG-based autocorrelator with a speaker-driven retroreflector in the fundamental beam arm [13].

At zero time delay and the SFG phase-matching condition, we observe a series of sideband signals evenly distributed on both sides of the FDF beam using a white sheet of paper placed behind the BBO crystal [bottom, Fig. 1(a)]. Using an RG610 longpass filter, the fundamental beam, IR SCWL and the sideband signals are clearly exposed on an IR sensor card [top, Fig. 1(a)]. In Fig. 1(b), the sideband spectra at the UV-Vis region from 350–500 nm are labeled as $V_{\pm i}$ ($i = 1 - 4$). Other sideband spectra within the NIR wavelength range of 700–1000 nm that hide in the UV-Vis beams are also measured. Apart from the 800 nm fundamental and IR-SCWL pulses, three sideband signals (I_{+1}, I_{-1}, and I_2) are found to be collinear with V_2, V_{-3} and V_4 beams, respectively [Figs. 1(b) and 1(c), spectra; Fig. 1(a), photograph). The sidebands

$I_{\pm 1,2}$ are assigned to the CFWM processes directly generated by the interacting fundamental and IR-SCWL pulses [1]. We achieve further proof by using a 0.1 mm thick BK7 glass plate and measuring the CFWM signals of $I_{\pm 1}$ [Fig. 1(c)] with the same experimental condition. Notably, the sideband signals observed for BBO within the UV-Vis wavelength range [Fig. 1(b)] are not observed in the glass that is amorphous and cannot support SFG or SHG generation for SFGFWM in the same medium.

The angle dependences of the sideband intensities at I_1 (750 nm) and V_2 (375 nm) are measured by rotating the BBO crystal as shown in the insert of Fig. 2. The experimental results reveal that the signal generation of I_1 is nearly independent of the rotation angle. A slight decrease of the I_1 intensity is observed when the BBO crystal is rotated to the SFG phase-matching condition, where the V_2 signal sharply reaches its highest intensity (Fig. 2). We attribute this observation to the intensity borrowing that occurs in BBO to facilitate SFGFWM at some expense of the regular CFWM.

From the aforementioned experimental results, the following two independent CFWM processes can be identified as: (1) CFWM within 700–1000 nm, generated from the two incident pulses, (2) SFGFWM within 350–500 nm, generated from the SFG signal interacting with the FDF pulse. In the CFWM processes, the wavevectors of the up-($\mathbf{k}_{Um}$) and down-($\mathbf{k}_{Dm}$) converted signals obey the phase-matching conditions $\mathbf{k}_{Um} = (m+1)\mathbf{k}_1 - m\mathbf{k}_2$ and $\mathbf{k}_{Dm} = (m+1)\mathbf{k}_2 - m\mathbf{k}_1$, respectively [1,3], where ***mm*** is the beam order of the sideband signal, while $\mathbf{k}_1$ and $\mathbf{k}_2$ correspond to the fundamental and SCWL laser pulses in CFWM, or the FDF and SFG laser pulses in SFGFWM. If the noncollinear copropagation of the two incident beams is considered [1,14], the wavevector magnitude of the mth-order up-converted beam with an interaction angle θ for phase matching is given by

$$\mathbf{k}_{Um} = \left\{[(m+1)\mathbf{k}_1 + m\mathbf{k}_2]^2 - 4m(m+1)\mathbf{k}_1\mathbf{k}_2\cos^2\left(\frac{\theta}{2}\right)\right\}^{\frac{1}{2}}. \quad (1)$$

Figure 3 shows the experimental and calculated wavevectors for all the sideband signals in the cascaded processes using Eq. (1). The filled triangles are calculation results for CFWM under the phase-matching conditions. The two solid arrow lines denote the fundamental ($\mathbf{k}_1$) and IR-SCWL ($\mathbf{k}_2$) laser beams with an interaction angle of 6°. At the SFG phase-matching condition (0° rotation angle in Fig. 2), the second cascaded process SFGFWM is observed, suggesting that the nascent, much stronger SFG signal (compared with the IR-SCWL pulse) steps in to interact with the SHG-assisted FDF beam at 400 nm for cascaded FWM in the UV-Vis regime. The filled squares represent the calculation results of SFGFWM with an interaction angle of 3° that is half of 6° due to the SFG geometry, so the CFWM signal occurs in the direction of every other SFGFWM signal (dotted lines in Fig. 3). All the experimental results agree well with calculations corroborating the proposed signal generation mechanism in one nonlinear crystal medium.

With a blue bandpass filter, we measure the autocorrelation signals of the different-order SFGFWM sidebands. The pulse duration decreases as the order of the sideband signal increases (Fig. 4). The dashed curve represents the first-order SFGFWM signal V_{-1}, with the pulse duration fitted to ~50 fs assuming Gaussian

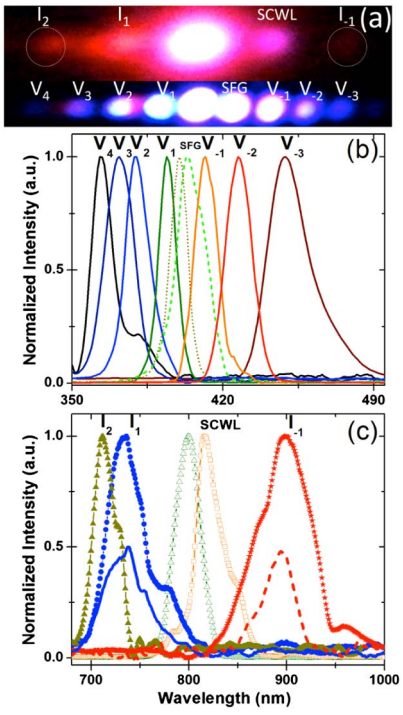

Fig. 1. (Color online) (a) Top, photograph of the CFWM sideband signals through an RG610 long-pass filter and viewed on an IR card. Bottom, photograph of the SFGFWM sideband signals on a sheet of white paper. (b) Normalized spectra of the SFGFWM sideband signals (solid curves), with the brightest FDF (dotted) and SFG (dashed) signals in the center. (c) Normalized spectra of the CFWM sideband signals. The solid triangles, circles and stars represent the CFWM signals generated in a 0.1-mm-thick BBO crystal. The solid and dashed lines display the corresponding signals generated in a 0.1-mm-thick BK7 glass plate (normalized to 0.5 intensity of the stronger BBO signals). The open triangles and squares show the 800 nm fundamental and IR-SCWL laser pulses, respectively.

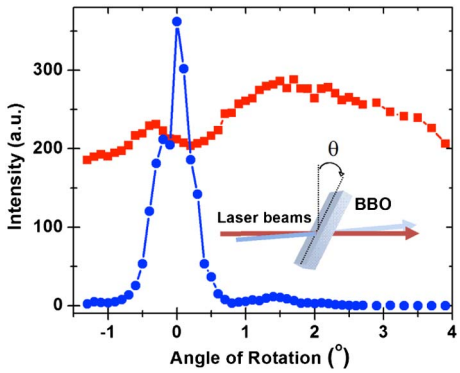

Fig. 2. (Color online) Angular dependence of the sideband signal intensity of I_1 at 750 nm (solid square) versus V_2 at 375 nm (solid circle). The rotation angle of 0° indicates the phase-matching condition for maximal SFG generation from the two incident laser pulses. The side view of the experimental setup using the 0.1 mm thin BBO crystal is shown as an inset.

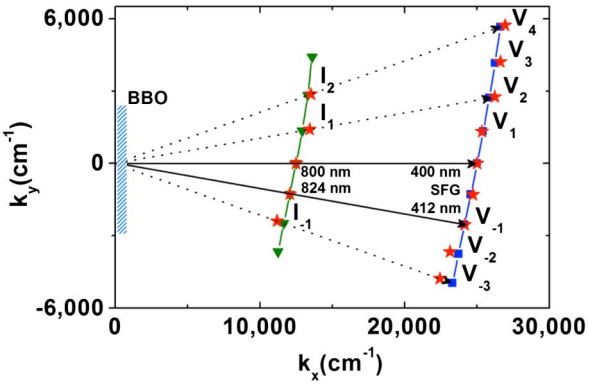

Fig. 3. (Color online) Calculated wavevectors of all the output beams in the observed pattern: solid stars, experimental results of CFWM and SFGFWM sidebands; solid triangles, calculated phase-matched sideband signals of CFWM with the interaction angle of 6°; solid squares, calculated phase-matched sideband signals of SFGFWM with the interaction angle of 3°. The solid curves are shown as a visual guide. The two solid arrow lines mark the fundamental and IR-SCWL pulses, and the dotted arrow lines connect the different-origin cascaded signals in the periodically collinear fashion. SFGFWM signals ($V_{\pm i}$) possess higher energy than CFWM signals ($I_{\pm i}$), hence are located at the right side of the figure corresponding to higher wavenumbers.

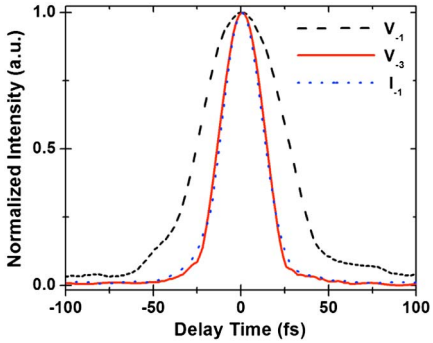

Fig. 4. (Color online) Temporal profiles of the concomitantly generated sideband signals. Self-compression is evident when comparing V_{-1} (dashed curve) with V_{-3} (solid) in SFGFWM, and with I_{-1} (dotted) in NIR CFWM. The increasingly higher-order product of the intervening fields dictates the compression effect, which correlates with naturally larger angular separation of the sideband signal with respect to the laser pump beams.

lineshape. Shorter pulse duration of ~30 fs is achieved for V_{-3}. With an RG610 longpass filter, the pulse durations of CFWM signals are measured. Figure 4 shows the I_{-1} signal with a pulse duration of ~30 fs that agrees with the self-compression effect at higher-order FWM signals generated by two fs laser pulses [15], but still broader than the Fourier transform limited pulse duration of ~15 fs dictated by the spectral bandwidth [see Figs. 1(b) and 1(c)].

As we increase the fundamental laser pulse energy to ~6 μJ/pulse, the periodic 2D multicolor lattice structure of SFGFWM is observed above and below the FDF beam (TOC figure) in parallel to the aforementioned one-dimensional sidebands. Further increase of the 800 nm pulse energy leads to more lines and brighter arrays across both dimensions around the FDF center (maximal intensity at time zero), indicating that the SFGFWM signal therein is possibly associated with multiple induced spatial solitons in nonlinear crystals [3,16].

In conclusion, we report two simultaneously generated CFWM processes in a 0.1 mm thick type-I BBO crystal using two fs laser pulses in a crossing geometry. The unique feature of this setup is the thin crystal with the weak broadband SCWL pulse acting in dual roles. The 700–1000 nm NIR CFWM signals are generated by the fundamental and the IR-SCWL pulses. The 350–500 nm SFGFWM signals, which are periodically collinear with the CFWM signals, arise from interactions between the SFG and FDF pulses in the thin BBO crystal. Self-compression is also observed in these cascaded sideband signals, particularly at higher orders but with reduced intensity. The energy conversion efficiency of the sideband signals is below 10% owing to the super thinness of BBO and relatively large crossing angle [3,15], but the spatial dispersion, broad spectral tunability and stability are the key to applying these sidebands to ultrafast spectroscopy. Such self-compressed broadband weak pulses are thus highly suitable to be used as probe beams in multicolor transient absorption or FSRS. We will report the application result with the crossing-angle dependence of the sideband in a future publication. These simultaneously generated and spatially separated sideband signals offer versatile broadband laser sources to conduct FSRS and other challenging time-resolved electronic and vibrational spectroscopy in one convenient lab setting.

This work is supported by the Oregon State University (OSU) faculty startup research fund and the College of Science (COS) venture fund award to C. Fang.

References

1. H. Crespo, J. T. Mendonca, and A. Dos Santos, Opt. Lett. **25**, 829 (2000).
2. J. Darginavicius, G. Tamošauskas, A. Piskarskas, and A. Dubietis, Opt. Express **18**, 16096 (2010).
3. J. Liu and T. Kobayashi, Sensors **10**, 4296 (2010).
4. J. Liu, J. Zhang, and T. Kobayashi, Opt. Lett. **33**, 1494 (2008).
5. E. Matsubara, T. Sekikawa, and M. Yamashita, Appl. Phys. Lett. **92**, 071104 (2008).
6. H. Matsuki, K. Inoue, and E. Hanamura, Phys. Rev. B **75**, 024102 (2007).
7. M. Zhi and A. V. Sokolov, Opt. Lett. **32**, 2251 (2007).
8. V. Couderc, A. Tonello, C. Buy-Lesvigne, P. Leproux, and L. Grossard, Opt. Lett. **35**, 145 (2010).
9. J. Fan, A. Migdall, and L. J. Wang, Opt. Express **15**, 7146 (2007).
10. S. Gao and X. Xiao, Opt. Commun. **285**, 784 (2012).
11. R. M. Hochstrasser, Proc. Natl. Acad. Sci. USA **104**, 14190 (2007).
12. R. R. Frontiera, C. Fang, J. Dasgupta, and R. A. Mathies, Phys. Chem. Chem. Phys. **14**, 405 (2012).
13. J. A. I. Oksanen, V. M. Helenius, and J. E. I. Korppi-Tommola, Rev. Sci. Instrum. **64**, 2706 (1993).
14. J. T. Mendonca, H. Crespo, and A. Guerreiro, Opt. Commun. **188**, 383 (2001).
15. R. Weigand, J. T. Mendonca, and H. M. Crespo, Phys. Rev. A **79**, 063838 (2009).
16. H. Zeng, J. Wu, H. Xu, and K. Wu, Phys. Rev. Lett. **96**, 083902 (2006).